# Charge and spin ordering in LiMn$_2$O$_4$

Izumi Tomeno

*Environmental Engineering and Analysis Center, Corporate Research & Development Center, Toshiba Corporation, Saiwai-ku, Kawasaki 212-8582, Japan*

Yusuke Kasuya* and Yorihiko Tsunoda

*School of Science and Engineering, Waseda University, Shinjuku-ku, Tokyo 169-8555, Japan*

X-ray diffraction, neutron diffraction, and susceptibility measurements were performed on $^7$LiMn$_2$O$_4$ powder specimen. The Jahn-Teller lattice distortion induces a phase transition from cubic to orthorhombic structure at $T = 283.5$ K on cooling. A series of well-defined magnetic Bragg peaks appears below $T_N = 65$ K. A complete charge ordering of Mn$^{3+}$ and Mn$^{4+}$ ions in the superlattice structure promotes the antiferromagnetic long-range order. The absence of a magnetic diffuse peak indicates that a magnetic frustration is removed from LiMn$_2$O$_4$ at low temperatures. The dynamics of the lithium ions are also discussed on the basis of the Debye-Waller factor.

## I. INTRODUCTION

Lithium-manganese oxide, LiMn$_2$O$_4$, is a promising candidate for application as cathode material in rechargeable lithium-ion batteries.[1,2] Environmentally and economically, LiMn$_2$O$_4$ is more suitable for Li batteries than is the popular product, LiCoO$_2$. Above 290 K LiMn$_2$O$_4$ has a cubic spinel structure in which the Li ions occupy the tetrahedral $A$ site, and the Mn ions occupy the octahedral $B$ site. The charge neutrality for LiMn$_2$O$_4$ requires that a ratio of Mn$^{3+}$ to Mn$^{4+}$ ions should be one to one. The presence of Mn$^{3+}$ ions in the $B$ site induces a first-order Jahn-Teller phase transition at about 280 K on cooling.[3] The Jahn-Teller distortion is relatively small, because Mn$^{4+}$ ions do not contribute anything to the Jahn-Teller transition.[3–5] The phase transition close to room temperature is harmful to the rechargeable battery. The partial substitution of Li for Mn depresses the Jahn-Teller transition temperature, due to the reduction of the Mn$^{3+}$ to Mn$^{4+}$ ratio.[4] Li-rich spinel Li$_{1+x}$Mn$_{2-x}$O$_4$ improves the rechargeable cycle performance at room temperature.[6]

The low-temperature (LT) crystal structure is still controversial. Yamada and Tanaka[3] proposed a mixture of the cubic and tetragonal phases below 280 K, using the x-ray diffraction study. Subsequent x-ray studies also indicated the coexistence of both phases below the Jahn-Teller transition temperature.[6–8] Wills, Raju and Greedan[9] also confirmed the existence of the tetragonal phase at 100 K using neutron diffraction. Recent x-ray and neutron diffraction studies, however, supported the orthorhombic symmetry.[10–13] Furthermore, electron, x-ray, and neutron diffraction measurements revealed the existence of the superlattice reflections in the LT phase.[10–13] Rodríguez-Carvajal *et al.*[10] found that the LT phase possesses space group symmetry $Fddd$. The unit cell in the LT phase is written as $3a \times 3b \times c$, where $a$, $b$, and $c$ are the lattice constants for the pseudocubic spinel.[11] They pointed out a partial charge ordering of Mn$^{3+}$ and Mn$^{4+}$ ions below 280 K. Hayakawa *et al.*[12] found that the orthorhombic phase finally changes to the tetragonal phase at 65 K on cooling.

Besides, the magnetism in LiMn$_2$O$_4$ is the subject of much controversy.[7–9,14–19] The existence of the spin-glass behavior is a point in question.[15,16] The inverse susceptibility $\chi^{-1}$ starts to deviate from linearity on cooling at temperatures ranging from 70 to 40 K.[8,16–18] Sugiyama *et al.*[18] reported the existence of an antiferromagnetic phase below 40 K by means of $^7$Li-NMR measurements. However, Oohara, Sugiyama, and Kontani[19] observed the absence of a magnetic long-range order even at 8 K in their neutron diffraction experiment. Instead, they found an antiferromagnetic diffuse peak below 100 K. They concluded that a geometrical frustration is responsible for the diffuse peak in LiMn$_2$O$_4$. Recently Wills, Raju, and Greedan[9] found that the magnetic Bragg peaks appear in the background of the magnetic diffuse peak in the range between 10 and 65 K. They concluded that a significant fraction of the spins remains disordered at 10 K.

Here, we investigate the structural and magnetic nature of $^7$LiMn$_2$O$_4$ using x-ray, neutron diffraction, and susceptibility measurements. X-ray diffraction shows that the LT phase is orthorhombic. Neutron diffraction indicates that the appearance of superlattice reflections in the LT phase is characterized by the first-order phase transition. Our specimen has magnetic features that distinguish it from the others.[7–9,14–19] Neutron-diffraction measurements clearly indicate an existence of the magnetic long-range order below 65 K. The transition at 65 K slightly changes the susceptibility vs temperature relationship. Scattering amplitude of Li ion is too small for x-ray diffraction, whereas neutron scattering amplitude for Li nuclei is rather large. We also discuss briefly the mobility of the Li ions using neutron scattering data.

## II. EXPERIMENTAL PROCEDURE

The polycrystalline sample of $^7$LiMn$_2$O$_4$ was synthesized by a conventional ceramic technique. Stoichiometric mixtures of 99.5% enriched $^7$Li$_2$O$_4$ and Mn$_2$O$_3$ were calcined at 700 °C in air for 12 h, pulverized, and pressed into pellets. The pellets were then fired at 850 °C in oxygen atmosphere
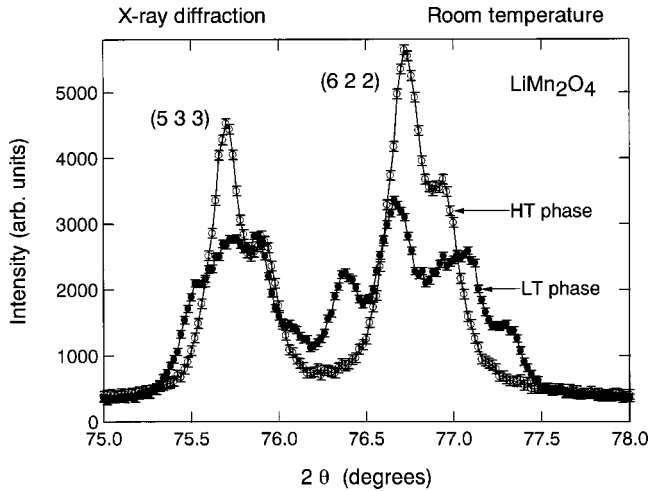
FIG. 1. X-ray diffraction patterns including (533) and (622) reflections on the HT and LT sides of the Jahn-Teller transition. These data are taken using Cu $K\alpha$ radiation at room temperature.

for 48 h with intermediate grinding. The $^7LiMn_2O_4$ sample was characterized on the LT and high-temperature (HT) sides of the Jahn-Teller transition by means of the powder x-ray diffraction. X-ray diffraction measurements were taken using Cu $K\alpha$ radiation with a pyrolytic graphite monochromator. Both phases are stabilized at room temperature due to a thermal hysteresis effect. The magnetic susceptibility was measured using a superconducting quantum interference device (SQUID) magnetometer in an applied field $H = 1000$ Oe from $T = 7-100$ K. Neutron diffraction measurements were performed using a conventional-type triple-axis spectrometer T1-1 installed at a thermal guide of JRR-3M, Tokai. The incident neutron wavelength $\lambda$ was 2.437 Å. The sample in a thin-wall vanadium can was enclosed in an aluminum vessel filled with helium gas. The aluminum vessel was attached to the cold finger of a refrigerator.

## III. RESULTS

### A. X-ray diffraction

Powder x-ray diffraction for the present sample indicated a single phase of the cubic spinel structure in the HT phase. Figure 1 shows the powder x-ray diffraction pattern including (533) and (622) peaks for the HT and LT phases at room temperature. The reflection indices used throughout the paper all refer to the cubic lattice. Subsidiary peak in the cubic phase is due to the Cu $K\alpha_2$ radiation. Figure 1 demonstrates that each peak for the (622) Bragg reflection splits into triplet in the LT phase due to the Jahn-Teller transition. Note that the central (622) peak position in the LT phase is apparently shifted to the lower angle with respect to the corresponding peak position in the HT phase. Furthermore, each peak intensity due to the $K\alpha_1$ radiation is roughly equal. Consequently, these findings lead to a conclusion that the crystalline structure of the present sample is orthorhombic in the LT phase. Lattice constants estimated from (622) peak are $a = 8.2324$ Å in the HT phase, and those for the LT phase are $a = 8.2402$ Å, $b = 8.2735$ Å, and $c = 8.188$ Å.
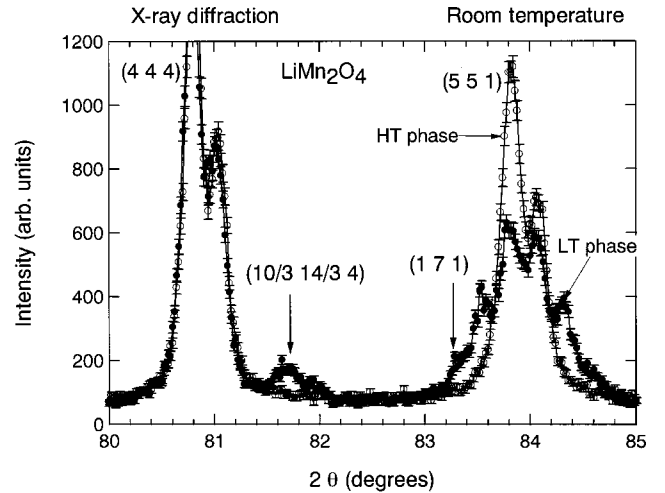


FIG. 2. Room-temperature x-ray diffraction patterns in the HT and LT phases. In addition to (444) and (551) Bragg peaks, the (10/3 14/3 4) and (171) superlattice reflections appear in the LT phase.

A series of weak superlattice reflections appears in the LT phase. Figure 2 demonstrates the existence of the (10/3 14/3 4) and (171) superlattice reflections. The observed superlattice reflection positions in the x-ray diffraction pattern are in good agreement with the data reported by Oikawa et al.[13] A comparison is made with the neutron diffraction results in III C.

### B. Magnetic susceptibility

Figure 3(a) plots the magnetic susceptibility $\chi$ for $LiMn_2O_4$ as a function of temperature. Our $\chi$ values in the observed temperature range are roughly equal to the values for the stoichiometric sample reported by Shimakawa, Numata, and Tabuchi.[8] The $\chi^{-1}$ vs temperature plot in Fig. 3(b) clearly show anomalies around $T' = 40$ K and $T_N = 65$ K. On cooling, $\chi^{-1}$ deviates slightly from a linearity at $T_N = 65$ K, and changes markedly at $T' = 40$ K. These results are quite different from previous reports.[7–9,14–19] The anomalies observed by previous authors are not so well defined as our data. The origins of anomalies at $T'$ and $T_N$ are discussed in a later section.

### C. Neutron diffraction

Neutron diffraction patterns in Fig. 4 demonstrate that the strongest nuclear superlattice peak appears at $2\theta = 64.1°$ ($Q = 2.74$ Å$^{-1}$) in the LT phase. The intensity of the superlattice peak at $2\theta = 64.1°$ is much higher than that for the (422) Bragg peak. The diffraction pattern for the $Fddd$ structure with $3a \times 3b \times c$ was calculated using the LAZY-PULVERIX program.[20] On the basis of these calculations, the (4/3 8/3 2) reflection makes up 88% of the superlattice peak intensity at $2\theta = 64.1°$, and the (5/3 1 3) reflection forms the remaining part. For convenience, we refer to the superlattice at $2\theta = 64.1°$ as the (4/3 8/3 2) reflection. Figure 5 depicts a comparison between the x-ray and the neutron diffraction results as a function of $Q$. Note that the (4/3 8/3 2) reflection
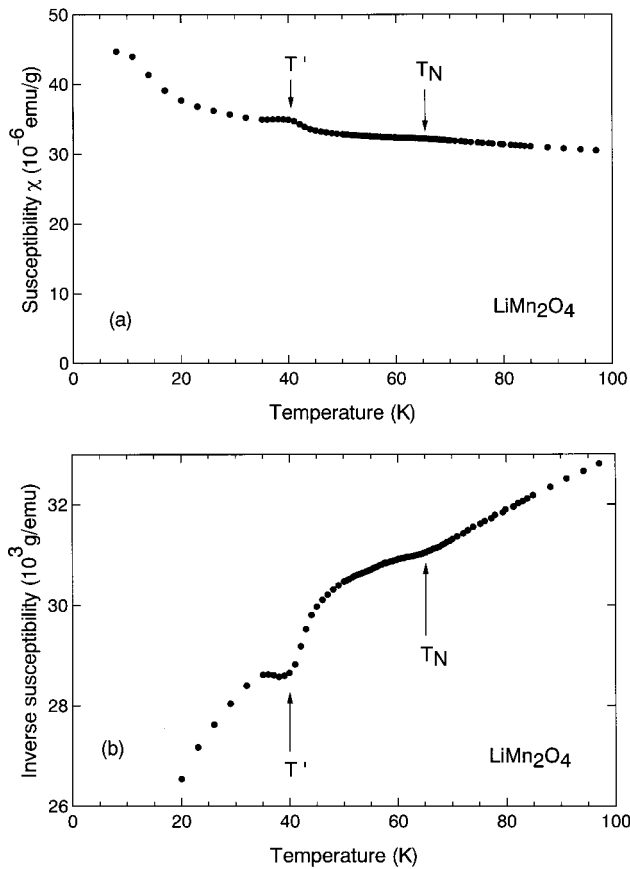
FIG. 3. (a) Temperature dependence of magnetic susceptibility $\chi$ for $^7$LiMn$_2$O$_4$ sample measured at H=1000 Oe. (b) Detail of inverse susceptibility $\chi^{-1}$.

at $Q=2.74\,\text{Å}^{-1}$ is missing in the x-ray diffraction pattern. In contrast, the x-ray data clearly show that the (2/3 10/2 0) superlattice reflection appears in the LT phase at $Q=2.59\,\text{Å}^{-1}$ ($2\theta=37.04°$). The calculated intensities for the *Fddd* structure can account for the lack of the correspon-
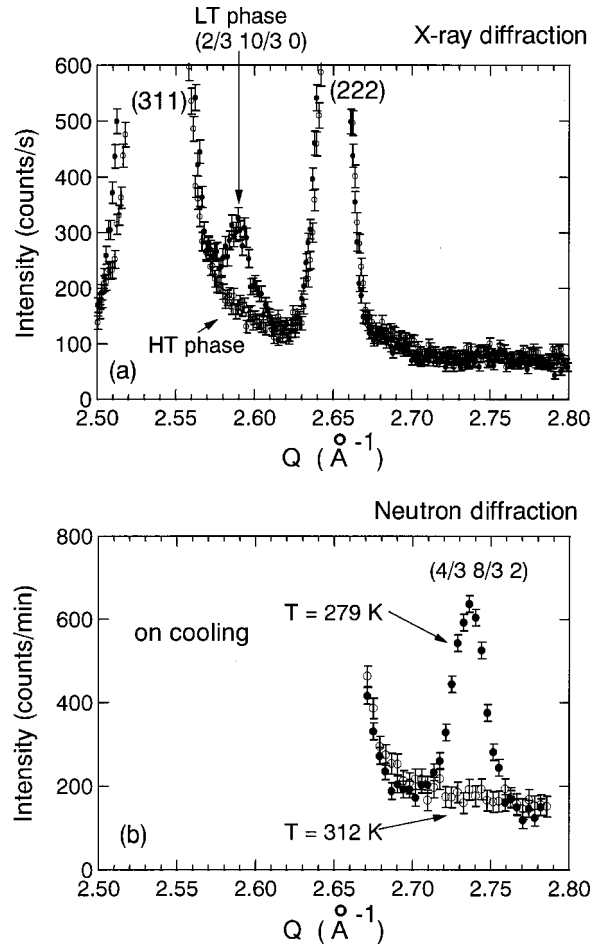


FIG. 5. Comparison of x-ray and neutron diffraction data as a function of $Q$. The superlattice reflection at $Q=2.74\,\text{Å}^{-1}$ in (b) neutron diffraction pattern is missing in (a) X-ray diffraction pattern. X-ray diffraction data were taken at room temperature.
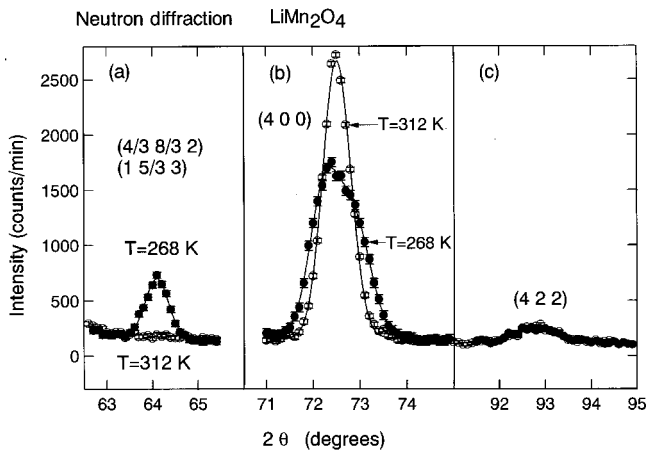


FIG. 4. Expanded neutron scattering pattern for (a) the superlattice reflection at $2\theta=64.1°$, (b) (400) Bragg peak, and (c) (422) Bragg peak. Open and closed circles refer to the data taken at 312 and 268 K, respectively. The superlattice reflection in (a) disappears completely at 312 K. The lines are Gaussian fits.
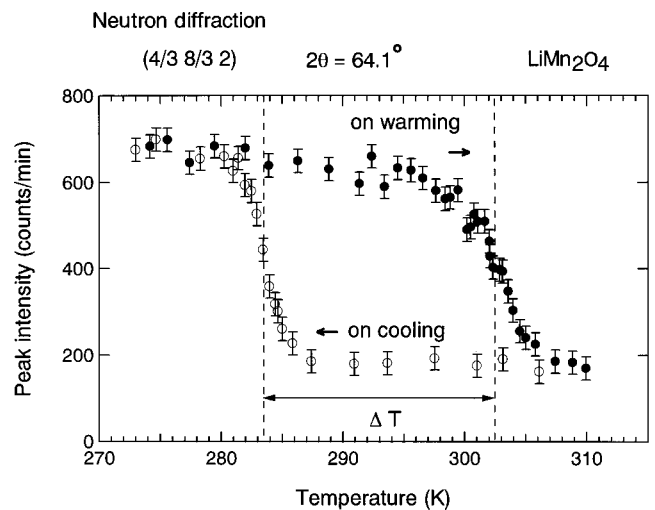


FIG. 6. The thermal hysteresis for the nuclear peak intensities at $2\theta=64.1°$.
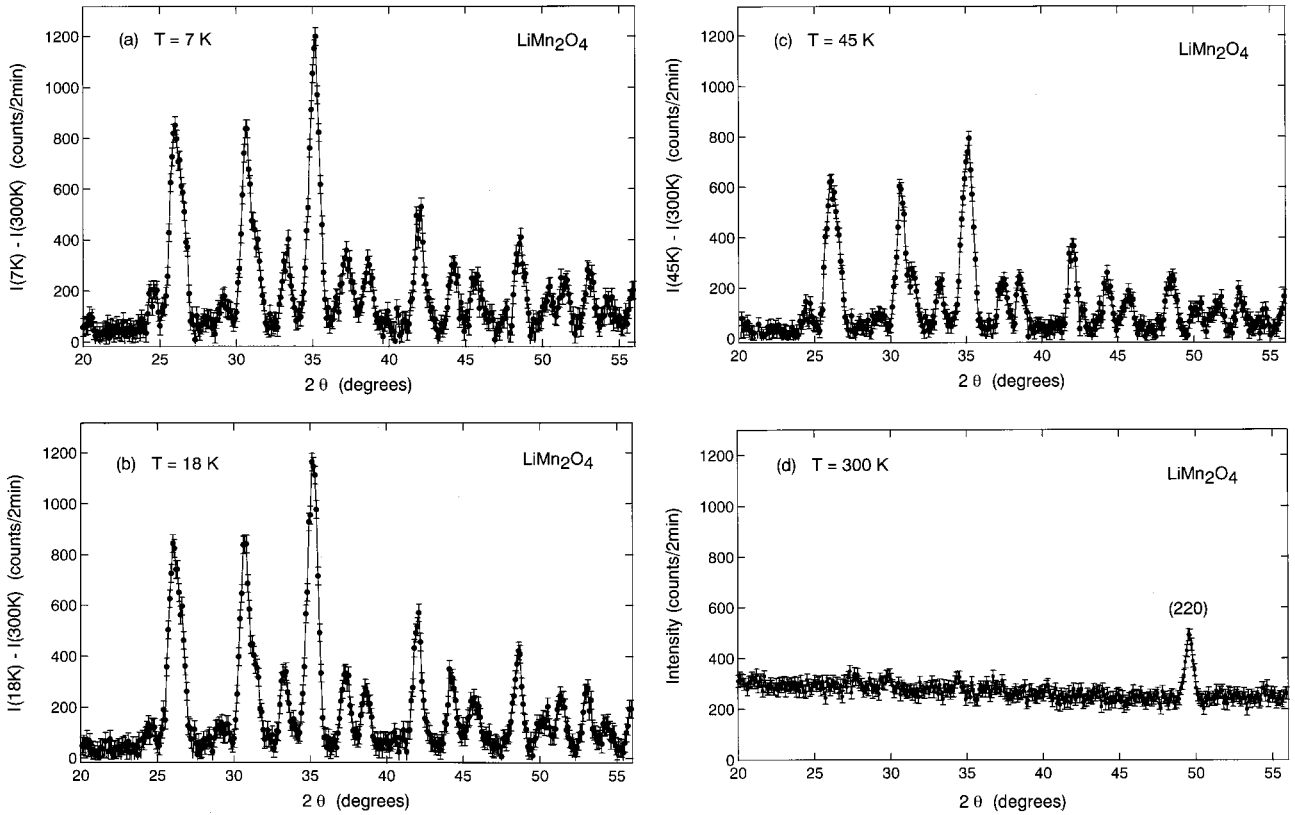
FIG. 7. Neutron diffraction patterns for $LiMn_2O_4$ at several temperatures. In (a), (b), and (c), the data at 300 K are subtracted from the data at each temperature.

dence with the superlattice reflections between x-ray and neutron diffraction measurements.

Figure 6 shows that the (4/3 8/3 2) peak intensity clearly reflects the characteristics of the first-order phase transition. The broken lines in Fig. 6 represent the Jahn-Teller transition temperature where the superlattice peak intensity at $2\theta = 64.1°$ reaches a 50% maximum. The Jahn-Teller transition temperature is 283.5 K on cooling and 302.5 K on warming, indicating the transition temperature interval $\Delta T = 19$ K. The $\Delta T$ value for the present sample is larger than the value $\Delta T = 13$ K deduced from resistivity measurements by Rousse et al.[11] and $\Delta T = 12$ K by Shimakawa, Numata, and Tabuchi.[8] The Jahn-Teller transition temperature on warming for the present sample is in good agreement with the value reported by these authors.[8,11] The integrated intensity ratio of the (4/3 8/3 2) to the (400) Bragg peak is found to be 0.266 for the present results shown in Fig. 5. The present integrated intensity ratio 0.266 is larger than the calculated intensity ratio 0.182 using the LAZY-PULVERIX program.[20] Furthermore, the corresponding peak height ratio 0.345 for the present result is considerably larger than the ratio 0.28 reported by Rodríguez-Carvajal et al.[10] and the ratio 0.22 reported by Oikawa et al.[13] Consequently these comparisons strongly suggest that the $LiMn_2O_4$ sample used in this study undergoes a complete transformation to the charge-ordering state below the Jahn-Teller transition temperature.

Figure 7 shows neutron diffraction patterns obtained at various temperatures. The data at 300 K were subtracted to reveal the magnetic component clearly. The room tempera-

ture data include the (220) nuclear Bragg peak at $2\theta = 49.5°$. There exist many sharp peaks at low temperatures. Most of them are magnetic in origin because they are temperature-dependent, as shown below. The magnetic peak widths are comparable to the (220) nuclear peak width. Consequently these results indicate the existence of a magnetic long-range order for this system. However, an attempt to index these peaks systematically was unsuccessful. The magnetic structure of $LiMn_2O_4$ would be incommensurate with the lattice periodicity.

Figure 7 shows the absence of the magnetic diffuse peak in temperature range between 7 and 65 K. The present results exhibit a sharp contrast to the existence of the magnetic diffuse peak at low temperatures reported by Oohara, Sugiyama, and Kontani[19] and by Wills, Raju, and Greedan.[9]

Figure 8 shows the temperature dependence of the magnetic scattering peak intensities at $2\theta = 26.1°$, $30.7°$, $33.2°$, and $35.2°$. Figure 8 also plots the nuclear superlattice reflection intensity at $2\theta = 24.6°$. All the magnetic peaks show similar behavior; the peak intensities attain the background counts at 65 K. From these data, the Néel temperature $T_N$ for $LiMn_2O_4$ is estimated to be 65 K. The existence of $T_N$ can account for one of the anomalies in the susceptibility $\chi$ shown in Fig. 3. In spite of more remarkable anomalies in $\chi$ at $T' = 40$ K, there is no marked difference in diffraction patterns between 18 and 45 K [Figs. 8(b) and 8(c)]. We also carefully studied the temperature dependence of magnetic peak intensities around 40 K. The peak intensities slightly
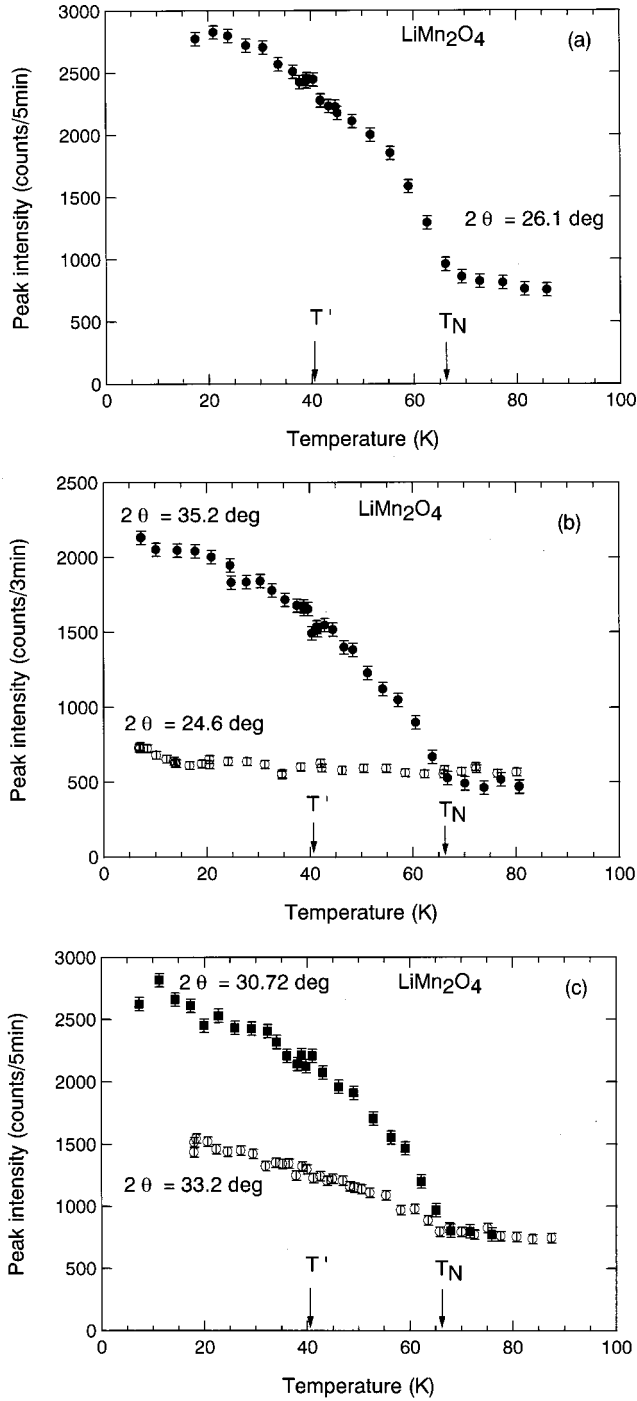
FIG. 8. Temperature dependence of magnetic peak intensities.

increase discontinuously at $T' = 40$ K on cooling. Thus the anomaly at $T' = 40$ K seems not to be magnetic in origin.

Figure 9 shows the temperature dependence of the $\theta$-$2\theta$ scans of the several nuclear Bragg reflections. The (11/3 3 1) and (7/3 3 3) superlattice reflections appear on the lower tail of the (422) peak in Fig. 9(c). The LT phase produces a split between (333) and (511) reflections. The calculated intensity shows that the observed peak in Fig. 9(d) is entirely due to the (333) reflection. The background near the (333) peak in Fig. 9(d) becomes slightly high at 150 K, suggesting the effect of the superlattice reflections such as (10/3 10/3 2),

(14/3 2 2), and (7/3 11/3 3). The $\theta$-$2\theta$ scans in Fig. 9 are fitted by the solid curves using Gaussian peaks and a background linear in $2\theta$.

Figure 10 shows the temperature dependence of the integrated intensities $I(hkl)(T)$. Here, $I(hkl)(T)$ are estimated by $WI_0$, where $W$ and $I_0$ are the fitted peak-width and peak-height parameters, respectively. The integrated intensity for each reflection decreases with increasing temperature. The integrated intensity is proportional to the square of the structure factor. In principle, the Bragg reflections in the LT phase should be expressed in terms of the structure factor for the orthorhombic phase. In practice, the essential feature of Bragg reflections in the cubic phase is still maintained in the LT phase. For the sake of simplicity, we analyze the integrated intensities using the structure factors $F(hkl)$ for the cubic phase of LiMn$_2$O$_4$. The structure factors squared are given by

$$[F(220)]^2 = 4b_{Li}^2 \exp[-2W_{Li}(220)], \qquad (1)$$

$$[F(331)]^2 = \{\sqrt{2}b_{Li}\exp[-W_{Li}(331)] \\ - 4b_{Mn}\exp[-W_{Mn}(331)]\}^2, \qquad (2)$$

$$[F(442)]^2 = 4b_{Li}^2 \exp[-2W_{Li}(422)], \qquad (3)$$

$$[F(333)]^2 = \{\sqrt{2}b_{Li}\exp[-W_{Li}(333)] \\ + 2b_{Mn}\exp[-W_{Mn}(333)]\}^2, \qquad (4)$$

where $b_{Li}$ and $b_{Mn}$ are the scattering lengths of $^7$Li and $^{55}$Mn, $-0.220 \times 10^{-12}$ cm and $-0.373 \times 10^{-12}$ cm, respectively; $\exp[-2W_{Li}(hkl)]$ and $\exp[-2W_{Mn}(hkl)]$ are the Debye-Waller factors for $^7$Li and $^{55}$Mn, respectively. The oxygen ions have no effect on these reflections. Note that both (220) and (422) Bragg peaks entirely come from the Li ions at the $A$ site. The Mn ions make a major contribution to the (331) and (333) reflections. The Li ions have a considerable effect on the (333) reflection. The Debye-Waller factor $\exp[-2W_x(hkl)]$ is given by

$$\exp[-2W_x(hkl)] = \exp[-\langle u_x(hkl)^2 \rangle Q^2], \qquad (5)$$

where $\langle u_x(hkl)^2 \rangle$ is the mean-square oscillation amplitude of the $x$ atoms along the scattering vector $Q$. The amplitude $\langle u_x(hkl)^2 \rangle$ is proportional to temperature for a normal lattice as long as an anharmonic effect is neglected. Here we introduce an average Debye-Waller factor for each reflection. The curves in Fig. 10 are least-squares fits to the data with the equation

$$I(khl)(T) = I(hkl)(0)\exp[-a(hkl)TQ^2]. \qquad (6)$$

The parameters $a(220)$ and $a(422)$ accurately correspond to $\langle u_{Li}(220)^2 \rangle / T$ and $\langle u_{Li}(422)^2 \rangle / T$, respectively. The estimated $a(hkl)$ values are given in Table I. Values for $a(220)$ and $a(422)$ are higher than those for $a(331)$ and $a(333)$. The observed relationships indicate that the displacement of the Li ions in LiMn$_2$O$_4$ is significantly larger than that for the Mn ions. Higher values for $a(220)$ and $a(422)$ are due to the light Li mass. The $a(333)$ result suggests that $a(hkl)$ is
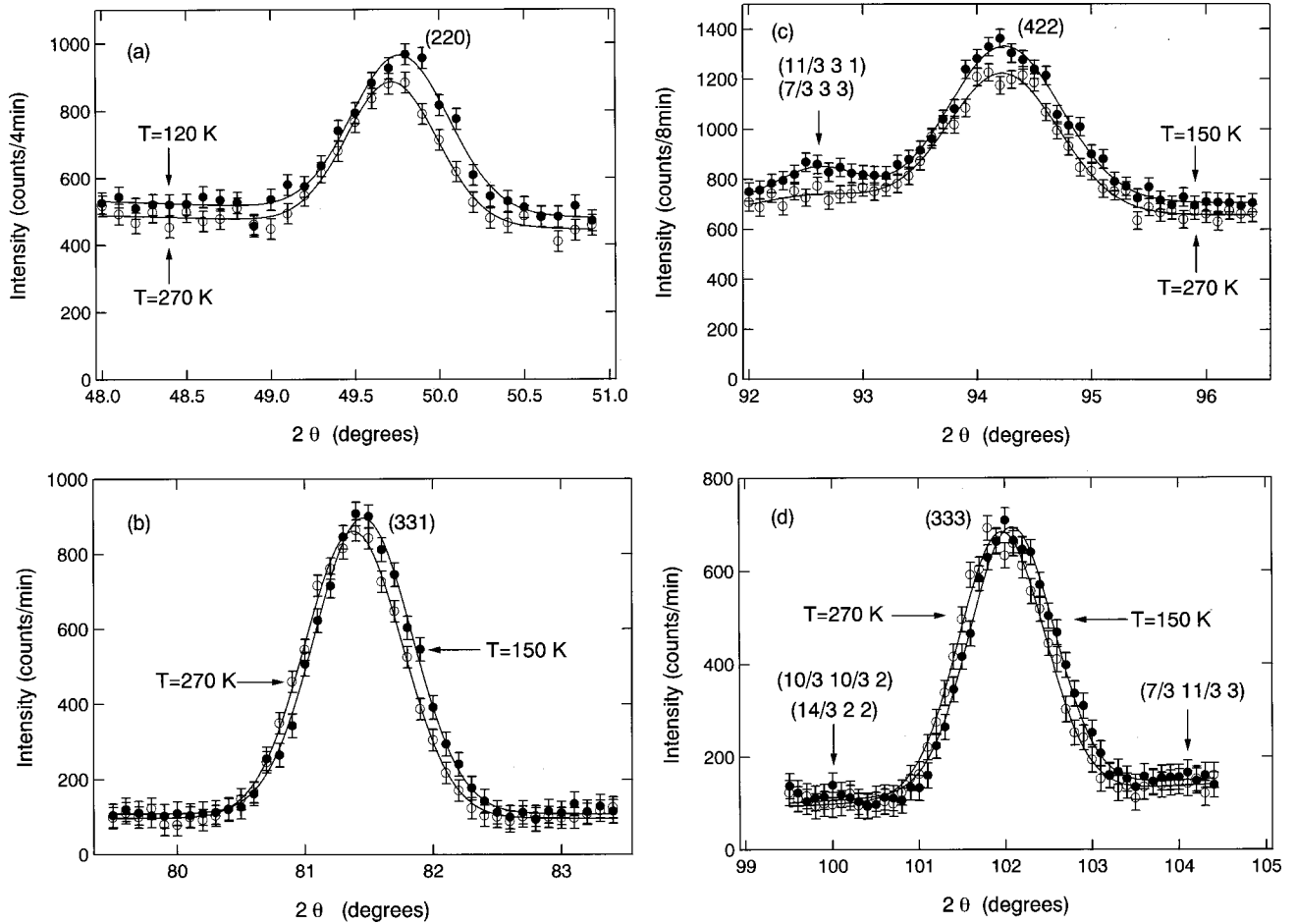
FIG. 9. Temperature dependence of nuclear peak intensities. The $\theta$-$2\theta$ scans are fitted by the solid curves using Gaussian peaks and a background linear in $2\theta$.

small in the $\langle 333 \rangle$ direction. The negative value for $a(333)$ may be due to systematic errors.

## IV. DISCUSSION

### A. Charge ordering

The octahedral $B$ site in spinel forms the network of the corner-sharing tetrahedra. One of the most extensively studied charge-ordering phenomena is the Verwey transition at $T_V = 123$ K in magnetite $Fe_3O_4$, where a charge ordering of $Fe^{3+}$ and $Fe^{4+}$ ions occurs at the $B$ site in the cubic inverse spinel structure.[21] Anderson[22] has pointed out that a short-range charge ordering persists above $T_V$ at the $B$ site in $Fe_3O_4$ to minimize the intersite Coulomb energy. Similarly, two $Mn^{3+}$-$Mn^{4+}$ pairs should occupy each tetrahedron even in the HT phase of $LiMn_2O_4$. In view of this, a doubled periodicity seems favorable to the $Mn^{3+}$-$Mn^{4+}$ charge balance in the LT phase. A tripled periodicity for $LiMn_2O_4$ slightly disturbs the short-range charge ordering in order to maintain the charge neutrality. The tripled superlattice requires an extra Coulomb energy compared with the doubled periodicity condition. The Jahn-Teller effect distorts the $Mn^{3+}O_6$ octahedra and simultaneously aligns the $3d_z^2$ orbital in the elongated $b$ axis. On the other hand, the $Mn^{4+}O_6$ oc-

tahedra practically remain undistorted. The charge ordering in the LT phase is directly associated with the systematic arrangement of the distorted and undistorted $MnO_6$ octahedra. Consequently, the strong intensity for the (4/3 8/3 2) superlattice reflection suggests that the Jahn-Teller distortion gives rise to the orbital ordering at the $Mn^{3+}O_6$ octahedra. The tripled periodicity suggests that the extra Coulomb energy is lower than the gain in reducing the elastic energy owing to the ordering of the distorted and the undistorted octahedra.

The charge ordering is measured by the intensity ratio of the (4/3 8/3 2) to the (400) Bragg peak. The $LiMn_2O_4$ sample used in this study has the highest ratio, as mentioned in Sec. III C. The charge ordering appears to be very sensitive to the sample synthesis condition. Oohara, Sugiyama, and Kontani[19] classified $LiMn_2O_4$ as the charge-disordered and magnetically frustrated system, by analyzing the magnetic diffuse peak. The observation of the well-defined superlattice, however, strongly suggests that the charge-ordered state is intrinsic to the LT phase of $LiMn_2O_4$.

### B. Antiferromagnetic long-range order

The present neutron diffraction results established that both charge and spin ordering occur at the Mn sites below
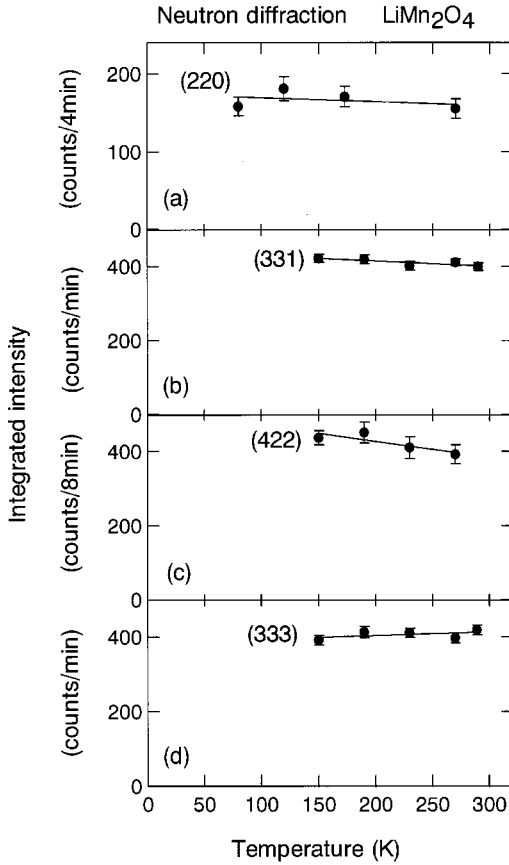
FIG. 10. Integrated intensity as a function of temperature. Solid lines are fits to the data with $I(hkl)(T) = I(hkl)(0)\exp[-a(hkl)TQ^2]$. The estimated $a(hkl)$ values are given in Table I.

$T_N = 65$ K. The same-valence ions at the $B$ site are expected to exhibit the geometrical frustration in the presence of the dominant nearest-neighbor antiferromagnetic interaction. The previous susceptibility data indicated the absence of the magnetic long-range order[8,14,17] or the existence of the spin-glass behavior.[15,16] These phenomena have been interpreted in the geometrical frustration scenario. The present results, however, disclose the existence of the antiferromagnetic long-range order below $T_N = 65$ K in LiMn$_2$O$_4$. The charge-ordered configuration in the tripled periodicity breaks the condition that four apexes for a single tetrahedron are magnetically equivalent sites.

The existence of the antiferromagnetic long-range order below $T_N = 65$ K is in marked contrast to the neutron scattering results reported by Oohara, Sugiyama, and Kontani.[19] They found the antiferromagnetic diffuse peak at $Q$

TABLE I. Parameters $a(hkl)$ used for the Debye-Waller factor ($10^{-5}$ K$^{-1}$Å$^2$)

| | |
|---|---|
| $a(220)$ | $6.5 \pm 12.3$ |
| $a(331)$ | $3.1 \pm 1.2$ |
| $a(422)$ | $7.2 \pm 3.2$ |
| $a(333)$ | $-1.5 \pm 1.6$ |

$= 1.4$ Å$^{-1}$ below 100 K, instead of the magnetic Bragg peaks. A series of magnetic peaks shown in Fig. 7 is roughly distributed in the range $1.15 < Q < 2.15$ Å$^{-1}$. The diffuse peak observed by Oohara, Sugiyama, and Kontani[19] covers the similar $Q$ region. A possible explanation is, therefore, that the suppression of the magnetic long-range order is ascribable to the imperfect charge-order at the structural phase transition. Wills, Raju, and Greedan[9] reported that the magnetic Bragg peaks coexist with the magnetic diffuse peak in the range between 10 and 65 K. A moderate reduction of the imperfect charge-order presumably gives rise to the magnetically partial ordered state reported by Wills, Raju, and Greedan.[9]

Many sharp magnetic peaks suggest that a complicated magnetic structure would be incommensurate with the superlattice periodicity. This is partly due to the presence of 144 Mn sites in a unit cell within $3a \times 3b \times c$, and partly due to the coexistence of Mn$^{3+}$ and Mn$^{4+}$ ions. The Mn$^{3+}$ ions at the $B$ site have the $t_{2g}^3$-$e_g^1$ orbital configuration ($S = 2$), whereas the Mn$^{4+}$ ions have the $t_{2g}^3$ configuration ($S = 3/2$). There are three distinguished superexchange interactions between nearest-neighbor Mn ion pairs: the 90° Mn$^{3+}$-O$^{2-}$-Mn$^{3+}$, the 90° Mn$^{3+}$-O$^{2-}$-Mn$^{4+}$, and the 90° Mn$^{4+}$-O$^{2-}$-Mn$^{4+}$, bonds. The Mn-Mn interaction for the former two linkages is antiferromagnetic, on the basis of the Goodenough-Kanamori rules.[23–25] In contrast, susceptibility measurements on manganese-oxide spinels containing Mn$^{4+}$ ions indicate that the 90° Mn$^{4+}$-Mn$^{4+}$ superexchange interaction is ferromagnetic.[7,14] The combination of these circumstances reflects the complicated spin structure in LiMn$_2$O$_4$.

The anomaly in the susceptibility $\chi$ at $T' = 40$ K is not magnetic in origin, in view of the temperature dependence of magnetic scattering peak intensities shown in Fig. 8. One possibility is that the structural phase transition is responsible for the anomaly in $\chi$ at $T'$. The study of x-ray diffraction by Hayakawa *et al.*[12] showed that LiMn$_2$O$_4$ undergoes two successive structural phase transitions; the intermediate orthorhombic $Fddd$ phase finally changes into the tetragonal $I4_1/amd$ phase at around 65 K with decreasing temperature. They determined the phase transition by observing the coincidence of the (400) and (040) reflection peak positions. The precise determination of the transition temperature appears to be difficult. We can explain consistently results for the magnetic scattering peaks and the susceptibility at $T'$ on the assumption that the structural phase transition occurs at 40 K for the present sample.

Another possibility is that the presence of Mn$_3$O$_4$ impurity contributes to the anomaly in $\chi$ at $T' = 40$ K. This possibility is based on the fact that $T' = 40$ K for LiMn$_2$O$_4$ is the vicinity of $T_C = 42$ K for a ferrimagnet Mn$_3$O$_4$.[26] Dwight and Menyuk[26] reported the temperature dependence of magnetization for Mn$_3$O$_4$ at $H = 1000$ Oe on cooling. Assuming that the change in $\chi$ at $T'$ is entirely due to the Mn$_3$O$_4$ impurity, our sample should be contaminated by the 0.1 wt. % Mn$_3$O$_4$ impurity. X-ray diffraction results, however, show that our sample is free from the Mn$_3$O$_4$ impurity. The discrepancy may be explained by the fact that the x-ray diffractometer cannot detect the low impurity level. In general, the neutron diffraction data are insensitive to the magnetic impurity on

the order of 0.1%. We would like to stress that our neutron scattering data show the intrinsic bulk properties of $LiMn_2O_4$, even if the 0.1% $Mn_3O_4$ impurity is responsible for the anomaly in $\chi$ at $T'$.

### C. Debye-Waller factor

The tetrahedral $A$ sites in spinel form a diamond lattice and share common faces with empty octahedral sites in the $\langle 111 \rangle$ direction. The Li ion amplitude becomes large toward the adjacent empty site, or the Li ion position slightly deviates from the centrosymmetric site. The configuration including the adjacent empty site has been found for the F ions in fluorite $CaF_2$ and for the O ions in actinide oxides $UO_2$ and $ThO_2$.[27–29] An anharmonic vibration in $CaF_2$, $UO_2$, and $ThO_2$ reduces the temperature dependence of the Debye-Waller factor $\exp[-2W(hhh)]$ in the $\langle hhh \rangle$ direction, compared with the normal behavior of $\exp[-2W(hkl)]$.[27–29] Furthermore, Eq. (5) does not hold for an anharmonic vibration: the $Q^4$ term also contributes to $W(hhh)$. The parameter $a(333)$ shown in Table I contains the contributions from

$W_{Li}(333)$ and $W_{Mn}(333)$. By analogy with the behavior of F and O ions in the fluorite structure, the small $a(333)$ value for $LiMn_2O_4$ may be attributable to the anharmonic Li ion motion.

### V. CONCLUSION

The Jahn-Teller transition transforms the cubic phase to the orthorhombic phase at 283.5 K on cooling. The existence of the strong (4/3 8/3 2) superlattice reflection is attributed to the charge ordering of $Mn^{3+}$ and $Mn^{4+}$ ions below the Jahn-Teller phase transition. Observations of magnetic Bragg peaks indicate that the antiferromagnetic long-range order exists below $T_N = 65$ K. The magnetic long-range order at low temperatures strongly depends on the charge ordering between $Mn^{3+}$ and $Mn^{4+}$ induced by the Jahn-Teller phase transition. The Debye-Waller factor in the $\langle 333 \rangle$ direction has weak temperature dependence, suggesting the existence of the anharmonic Li ion vibrations toward the adjacent empty site.

*Present address: Shimane Medical University, Izumo City, Shimane 693-8501, Japan.

[1] M. M. Thackeray, W. I. F. David, P. G. Bruce, and J. B. Goodenough, Mater. Res. Bull. **18**, 461 (1983).

[2] M. M. Thackeray, P. J. Johnson, L. A. de Picciotto, P. G. Bruce, and J. B. Goodenough, Mater. Res. Bull. **19**, 179 (1984).

[3] A. Yamada and M. Tanaka, Mater. Res. Bull. **30**, 715 (1995).

[4] A. Yamada, K. Miura, K. Hinokuma, and M. Tanaka, J. Electrochem. Soc. **142**, 2149 (1995).

[5] A. Yamada, J. Solid State Chem. **122**, 160 (1996).

[6] R. J. Gummow, A. de Kock, and M. M. Thackeray, Solid State Ionics **69**, 59 (1994).

[7] C. Masquelier, M. Tabuchi, K. Ado, R. Kanno, Y. Kobayashi, Y. Maki, O. Nakamura, and J. B. Goodenough, J. Solid State Chem. **123**, 255 (1996).

[8] Y. Shimakawa, T. Numata, and J. Tabuchi, J. Solid State Chem. **131**, 138 (1997).

[9] A. S. Wills, N. P. Raju, and J. E. Greedan, Chem. Mater. **11**, 1510 (1999).

[10] J. Rodríguez-Carvajal, G. Rousse, C. Masquelier, and M. Hervieu, Phys. Rev. Lett. **81**, 4660 (1998).

[11] G. Rousse, C. Masquelier, J. Rodríguez-Carvajal, and M. Hervieu, Electrochem. Solid-State Lett. **2**, 6 (1999).

[12] H. Hayakawa, T. Takada, H. Enoki, and E. Akiba, J. Mater. Sci. Lett. **17**, 811 (1998); H. Hayakawa, T. Takada, H. Enoki, and E. Akiba, Powder Diffr. **15**, 19 (2000); T. Takada, H. Hayakawa, H. Enoki, E. Akiba, H. Slegr, I. Davidson, and J. Murray, J. Power Sources **81-82**, 505 (1999).

[13] K. Oikawa, T. Kamiyama, F. Izumi, B. Chakoumakos, H. Ikuta, M. Wakihara, J. Li, and Y. Matsui, Solid State Ionics **109**, 35

(1998).

[14] G. Blasse, J. Phys. Chem. Solids **27**, 383 (1966).

[15] P. Endres, B. Fuchs, S. Kemmler-Sack, K. Brandt, G. Faust-Becker, and H.-W. Praas, Solid State Ionics **89**, 221 (1996).

[16] Y. Jang, F. C. Chou, and Y. Chiang, Appl. Phys. Lett. **74**, 2504 (1999).

[17] C. B. Azzoni, M. C. Mozzati, A. Paleari, D. Capsoni, and M. Bini, Z. Naturforsch., A: Phys. Sci. **53A**, 693 (1998).

[18] J. Sugiyama, T. Hioki, S. Noda, and M. Kontani, J. Phys. Soc. Jpn. **66**, 1187 (1997).

[19] Y. Oohara, J. Sugiyama, and M. Kontani, J. Phys. Soc. Jpn. **68**, 242 (1999).

[20] K. Yvon, K. Jeitschko, and E. Parthe, J. Appl. Crystallogr. **10**, pt. 1, 73 (1977).

[21] E. J. W. Verwey and P. W. Haayman, Physica (Amsterdam) **8**, 979 (1941); E. J. W. Verwey, P. W. Haayman, and F. C. Romejin, J. Chem. Phys. **15**, 181 (1947).

[22] P. W. Anderson, Phys. Rev. **102**, 1008 (1956).

[23] J. B. Goodenough, *Magnetism and the Chemical Bond* (Interscience Publishers, New York, 1963); Phys. Rev. **100**, 564 (1955).

[24] J. Kanamori, J. Phys. Chem. Solids **10**, 87 (1959).

[25] P. W. Anderson, in *Solid State Physics 14*, edited by F. Seitz and Turnbull (Academic Press, London, 1963), Chap. 2.

[26] K. Dwight and N. Menyuk, Phys. Rev. **119**, 1470 (1960).

[27] B. Dawson, A. C. Hurley, V. W. Maslen, Proc. R. Soc. London, Ser. A **298**, 289 (1967).

[28] B. T. M. Willis, Acta Crystallogr. **18**, 75 (1965).

[29] B. T. M. Willis, Proc. R. Soc. London, Ser. A **274**, 122 (1963); **274**, 134 (1963).